

STABILITY OF AXISYMMETRIC LIQUID BRIDGES

I. Martínez

E.T.S.I. Aeronáuticos, Universidad Politécnica de Madrid, Spain

ABSTRACT

A simple formulation and a compact set of graphic data are presented for the equilibrium shapes and stability limits of axisymmetric liquid bridges. The stability analysis is based on the bifurcation of static configurations and gives the minimum liquid volume a bridge can hold, and the breaking mode. The end supports considered are: equal discs, unequal discs, free edge plates and paraboloidal supports.

Keywords: liquid bridge, stability, capillarity, interfaces, microgravity.

1. INTRODUCTION

Small liquid volumes, partially attached to solid boundaries, naturally appear in a variety of applications, and some basic phenomena as capillary hysteresis are not yet fully understood. Levitation of large samples under reduced gravity, allows for a more detailed analysis to be performed, while orbiting platforms as Spacelab promise to provide the appropriate environment.

In this frame, this paper presents some theoretical results on the stability limits, what seems to be of great value in the understanding of other, less easily controlled, phenomena.

The modelling is quite simple: only equilibrium shapes are considered, satisfying Laplace equation of capillary pressure, that, in a dimensionless form, reads

$$K + P + Wr^2/2 - Bz = 0 \quad (1)$$

K being the local mean curvature at a point in the interface, P a constant related to the origin of pressures, W the imposed rotation Weber number, B the imposed Bond number due to a residual microgravity, and r and z the radial and axial coordinates. Explicit expressions for W and B will depend on the length chosen to nondimensionalize.

Two integration constants from the second order differential operator K , plus the constant P are to be

substituted by the three imposed boundary conditions: one at the solid contact at each end of the bridge, and the volume of liquid, which is supposed to be controlled.

Two different simplifying boundary conditions are considered (Figure 1): fixed end-points (liquid borders anchored at a sharp solid edge) and free end-points with fixed contact angle; the latter seems the less controllable assumption in practice.

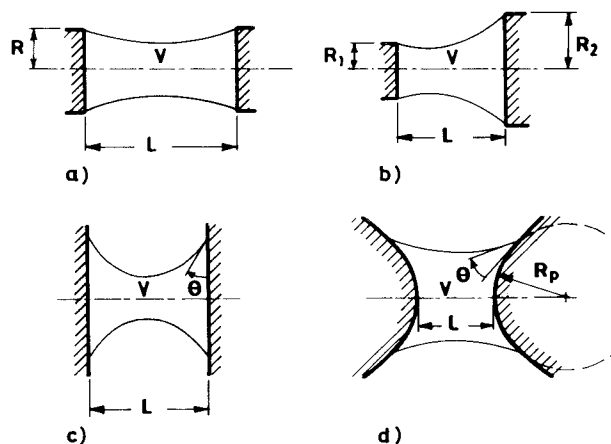


Figure 1. Bridge geometries considered: a) equal discs, b) unequal discs, c) free edge plates, d) paraboloidal supports.

Equilibrium shapes for axisymmetric bridges when $W = B = 0$ are pieces of Plateau's constant-curvature surfaces of revolution, what greatly reduces the effort to find the stability limit that here is just performed by plotting every possible equilibrium point in a volume-slenderness diagram and checking for the free energy of similar points to be a minimum (further insight is to be gained from the different cases described below in detail).

2. EQUAL DISCS

The disc radius R is taken as unit length and thus $W = \rho\Omega^2 R^3 / \sigma$ and $B = \rho g R^2 / \sigma$ in Eq. 1. Two additional nondimensional variables are introduced: the slenderness of the bridge $\lambda = L / (2R)$ and the volume $v =$

V/R^3 . The configuration is determined by the disc radius R , their separation L , and the volume V of liquid (see Figure 1a), and the relevant fluid properties are the density difference ρ and the interface tension σ with the surrounding fluid (a gaseous atmosphere or an outer liquid as in the Plateau tank technique).

In absence of rotation and gravity, i.e. for $W=B=0$, with $v=2\pi\Lambda$, the trivial solution of a cylindrical shape takes place, being stable when $0 \leq \Lambda \leq \pi$ as already known for more than a century. The cylinder is also the stable shape when a solid body rotation $W \neq 0$ exists, provided a combination $f(\Lambda, W) = 0$ is not exceeded; the exact expression for f was given in Ref. 1 and approaches $\Lambda = \pi(1 - W/2)$ for small W .

When an axial microgravity is present, i.e. for $B \ll 1$ with $W=0$ and $v=2\pi\Lambda$, the cylinder $r=1$ is no longer an equilibrium shape, deforming to (Ref. 2)

$$r = 1 + B \left(\frac{1}{\sin \Lambda} - \frac{\pi}{2\Lambda} \right) \sin \frac{\pi z}{\Lambda} \quad 0 \leq z \leq 2\Lambda \quad (2)$$

with a limit of stability $\Lambda = \pi [1 - (9B/4)^{3/2}]$ for small B , given in Ref. 3.

The whole volume-separation stability diagram in the absence of rotation and gravity was presented in Ref. 4, but if only slight volume departures from that of a cylinder are envisaged, i.e. for $W=B=0$ with $v-2\pi\Lambda \ll 1$, the combination $f(\Lambda, v)$ bounding the stability region can be approximated to $\Lambda = \pi [1 + (v-2\pi\Lambda)/4]$; this excess in volume forces the cylinder $r=1$ to deform to (Ref. 2)

$$r = 1 + \frac{v-2\pi\Lambda}{2\pi\Lambda} \frac{1-\cos \Lambda}{4\sin \Lambda - 2\cos \Lambda} \sin \frac{\pi z}{2\Lambda} \quad 0 \leq z \leq 2\Lambda \quad (3)$$

On the other hand, if an initial deformation is imposed on the cylinder in the case $W=B=0$ with $v=2\pi\Lambda$, a dynamical evolution will follow, except in the limiting case it coincides with the unstable equilibrium shapes described in Ref. 2 (Figure 2) that can be approximated by

$$r^2 = 1 + \left[\frac{4}{\sqrt{3}} \lambda^{1/2} (1-\lambda) \right] \sin \frac{\pi z}{\Lambda} \quad 0 \leq z \leq 2\Lambda \quad (4)$$

where $\lambda = 1 - \Lambda/\pi$. The square of r is used to extend the range of validity of Eq. 4 since it fully satisfies the $v = \text{const}$ constraint for any Λ .

In conclusion, the influence of the above perturbations on the well-known stability limit $\Lambda = \pi$ for a cylindrical bridge anchored at its edges is best visualized by the reduction they impose on the maximum attainable slenderness

$$\Lambda_{\max} = \pi \left[1 - \frac{W}{2} - \left(\frac{9}{4} B \right)^{3/2} - \frac{3}{16} a^2 + \frac{v-2\pi\Lambda}{4\pi} \right] \quad (5)$$

where a stands for the amplitude of a sinusoidal perturbation. Although Eq. 5 is just a linear approximation, it is worth noticing that the exact dependence on all the mentioned effects, assumed isolated, is known (Refs. 2 and 5). Further results concerning the celebrated C-mode rotational instab-

ility that may arise for $\Lambda < \sqrt{3}\pi/2$ can be found in Ref. 3.

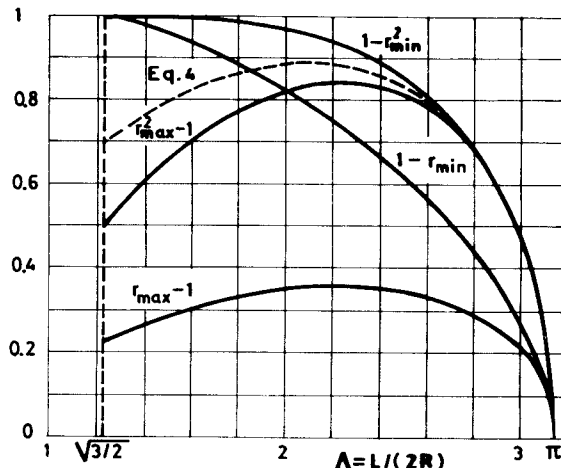


Figure 2. Extremal deviations from the cylinder $r=1$ corresponding to unstable equilibrium shapes of cylindrical volume $v=2\pi\Lambda$. Both the maximum and the minimum for the radius r and the cross-section r^2 are plotted versus the bridge slenderness Λ . The dashed line correspond to the approximation of Eq. 4.

3. UNEQUAL DISCS

Let w be the diameter ratio of the smaller to the larger diameter disc (Figure 1b); $w=1$ recovers the analysis for equal discs. The shape of the bridge $r=r(z)$ can best be described (in an internal coordinate system used for Plateau's curves) as $r=r(\alpha, \phi)$ and $z=z(\alpha, \phi)$, where α measures the curvature characterizing the curve, and ϕ serves to generate points along it. With the origin in a maximum and its ordinate as unit length, the expressions for the curve points (r, z) , the slope angle γ , and the volume v and surface area s up to this section are given by:

$$\left. \begin{aligned} r(\alpha, \phi) &= \sqrt{1 - \sin^2 \alpha \sin^2 \phi} \\ z(\alpha, \phi) &= \cos \alpha F(\alpha, \phi) + E(\alpha, \phi) \\ |\gamma(\alpha, \phi)| &= \arccos \frac{r + \cos \alpha / r}{1 + \cos \alpha} \\ v(\alpha, \phi) &= \frac{\pi}{3} \left[r \sqrt{(1-r^2)(r^2 - \cos^2 \alpha)} - z \cos \alpha + 2(1 + \cos \alpha)^2 E(\alpha, \phi) \right] \\ s(\alpha, \phi) &= 2\pi(1 + \cos \alpha) E(\alpha, \phi) \end{aligned} \right\} \quad (6)$$

where F and E are the alliptic integrals of the first and second class. The only Plateau curve not included in this formulation is the catenoid, but its study is much simple.

The aim is to know which of the several possible equilibrium shapes is the stable one (in some neighbourhood), for predefined values of R_1, R_2, L and V (radius of the discs, disc separation and liquid volume). The procedure is as follows; once $w=R_1/R_2$ fixed, a bidimensional scan in α and ϕ allows to compute the dimensionless parameters

$$\frac{L}{R_1+R_2} = \frac{z(\alpha, \phi') - z(\alpha, \phi)}{r(\alpha, \phi') + r(\alpha, \phi)} \quad (7)$$

$$\frac{V}{(R_1+R_2)^3} = \frac{v(\alpha, \phi') - v(\alpha, \phi)}{[r(\alpha, \phi') + r(\alpha, \phi)]^3} \quad (8)$$

$$\frac{S}{(R_1+R_2)^2} = \frac{s(\alpha, \phi') - s(\alpha, \phi)}{[r(\alpha, \phi') + r(\alpha, \phi)]^2} \quad (9)$$

with ϕ' given by the constrain in the disc-diameter ratio w

$$w = \frac{\sqrt{1 - \sin^2 \alpha \sin^2 \phi'}}{\sqrt{1 - \sin^2 \alpha \sin^2 \phi}} \quad (10)$$

If then $V/(R_1+R_2)^3$ is plotted versus $L/(R_1+R_2)$ as Figure 3 shows for $w=0.99$, a minimum-volume curve appears. Figure 4 is a summary of this stability limit, the most important from the practical point of view, for different disc-diameter ratios w (upper volume limits are dealt with in the same way).

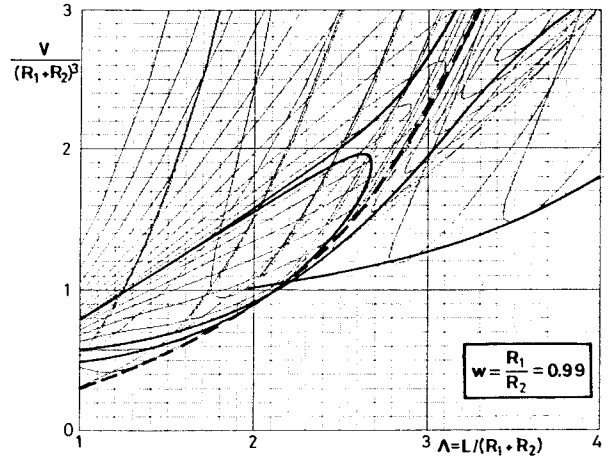


Figure 3. Volume-separation diagram for disc-diameter ratio $w=0.99$. Thin lines correspond to different Plateau curves ($\alpha=\text{const}$). Thick lines correspond to bridges with one angle at the disc edge equal to $\pi/2$. The dashed line is the stability limit.

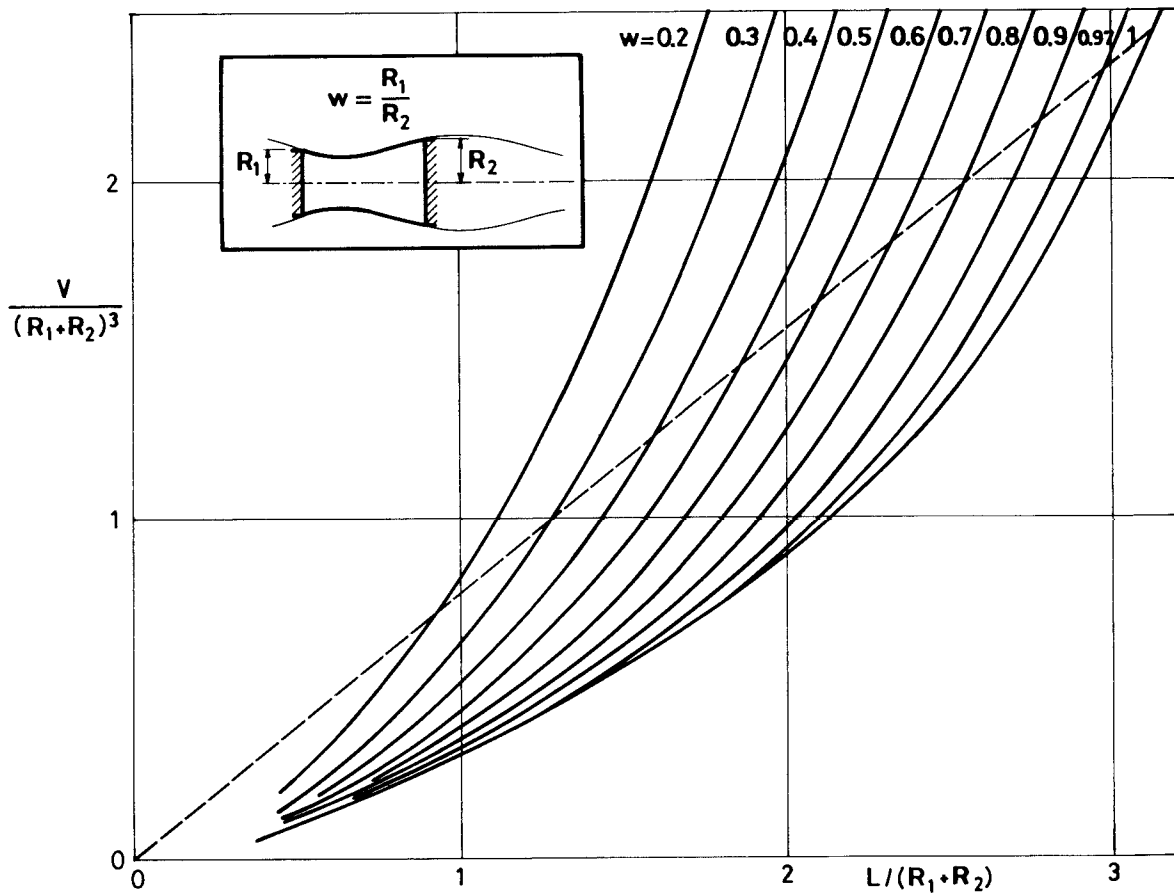


Figure 4. Stability limits for several disc-diameter ratios w , showing the minimum liquid volume for a bridge of span L . Dashed line corresponds to "cylindrical" configurations, i.e. $v=\pi(R_1+R_2)^2L/4$.

Normally, the local minimum in the volume will be the stability limit, but to verify that, (α, ϕ) couples of constant $L/(R_1+R_2)$ can be selected from the volume-separation diagram and its interface area $S/(R_1+R_2)^2$, equal to the nondimensional free energy of the system, plotted versus $V/(R_1+R_2)^3$. The true stability limit will become apparent, as shown in Figure 5, where the above-mentioned procedure has been followed for two cases, $\Lambda=1.5$ and $\Lambda=2.5$, with $w=0.99$ to compare with Figure 4.

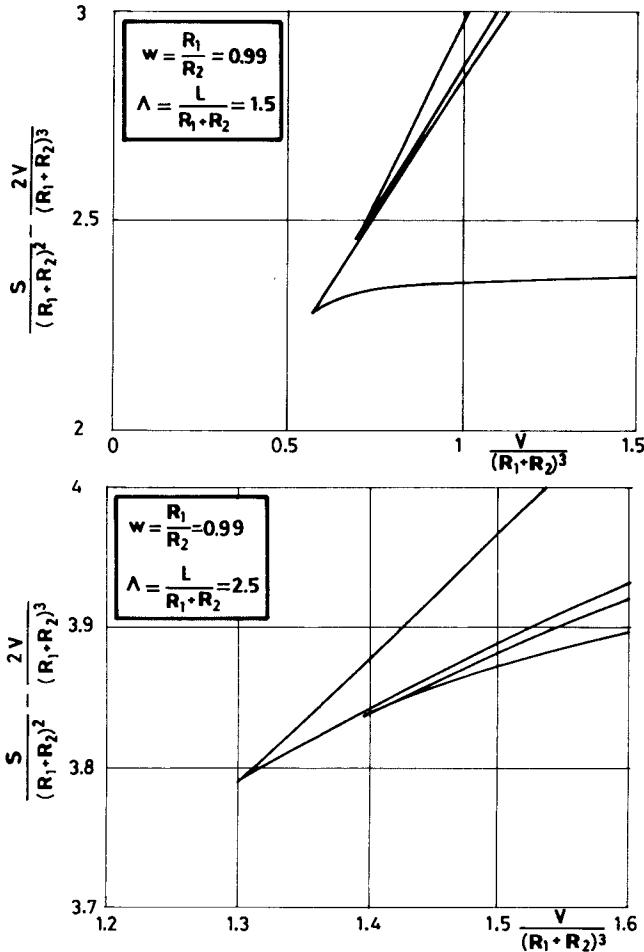


Figure 5. Free energy (interface area) S of a liquid bridge between discs of diameter-ratio $w=0.99$ versus volume V , for a constant separation Λ . The shift on the ordinates is just to enhance the graphic.

Other conclusions to be drawn from the analysis of unequal-disc configurations are that short bridges break with angles at both edges below $\pi/2$ whereas long bridges do it with one below and the other above $\pi/2$. Moreover, the breaking neck always forms near the smaller disc (it remains indetermined with equal discs). Finally, edge detachment for short bridges when decreasing the volume always take place at the larger disc.

Most of the above results can be easily understood if comparison is made with the equal-disc case in the special case $V=\pi L(R_1+R_2)^2/4$, corresponding to the cylindrical evolution $V=\pi R^2 L$ for equal discs. The bifurcation pattern is sketched in Figure 6

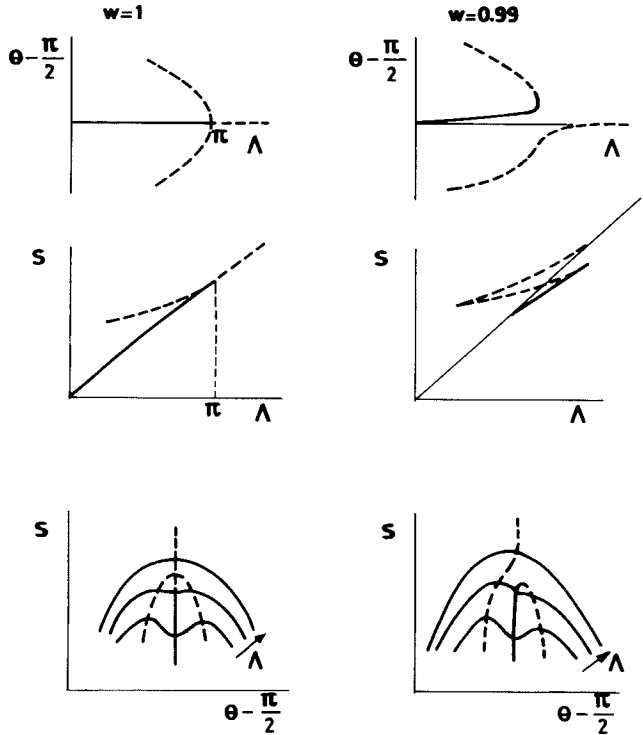


Figure 6. Comparison of the bifurcation at the stability limit for "cylindrical" bridges ($V=\pi L(R_1+R_2)^2/4$) between equal discs $w=1$ and unequal discs of diameter ratio $w=0.99$.

where the angle with the larger disc is taken as bifurcating variable. In some respect, this effect is similar to that of a small axial gravity for equal discs (the role of the bottom disc is here played by the smaller disc).

Finally, the difference in the bifurcation pattern at constant disc separation is illustrated in Figure 7, where the unstable symmetrical cusp found for $\Lambda>2.13$ with equal discs is seen to yield a new local minimum in the volume.

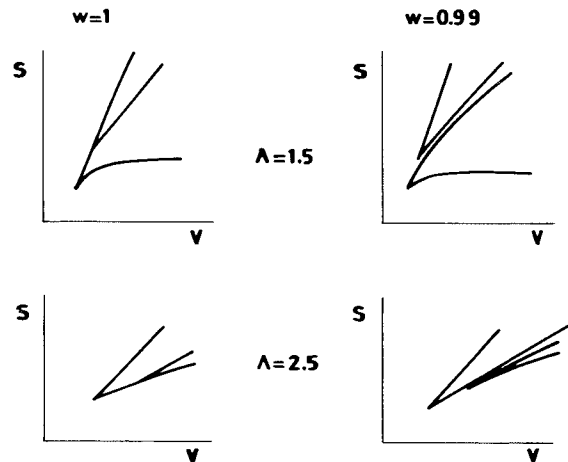


Figure 7. Free energy versus volume, showing the effect of a small difference in the diameter of the discs for constant disc separation $\Lambda=1.5$ and $\Lambda=2.5$.

4. FREE EDGE PLATES

The quasi-static modelling of a three phase line (at the intersection of the fluid-fluid interface with the solid boundary) as a constant contact-angle border seems rather poor and far from experimental evidence, but because of its simplicity it is a common assumption and will be followed here.

Using the only available length L as unity, the geometry rests specified in practice by giving the contact angle θ and the nondimensional volume V/L^3 (see Figure 1c). Since θ is the complementary of the slope angle γ given in Eq. 6, and due to its simple dependence on α and ϕ (not involving elliptical integrals) the procedure, though similar to that explained for unequal discs, can be carried out in a straightforward manner.

For a given θ , the maximum $\alpha \in (-\pi, 0)$ that can accommodate such a bridge is $\alpha_m = -2 \arctg \sqrt{\cos \theta}$, thus a simple scan on α is enough to draw the $(S/L^2, V/L^3)$ plot from which the stability limit is found. Notice that now S represents the effective interface area, $S = S_{liq-gas} - S_{liq-sol} \cos \theta$, coincident (in nondimensional variables) with the free energy of the system. This has been carried out in Figure 8 for two contact angles: 10 and 45 degrees.

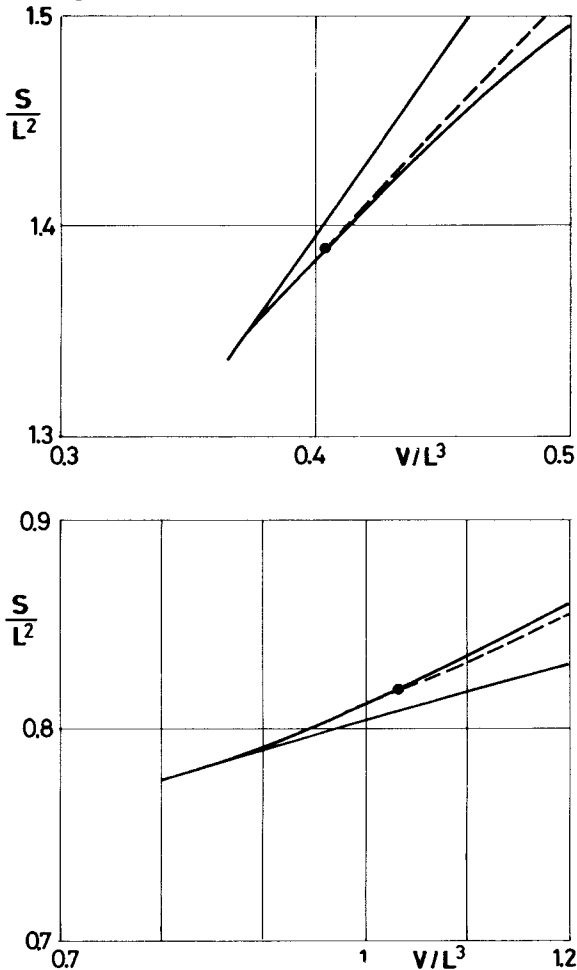


Figure 8. Free energy (effective interface area) versus volume for a free-edge bridge of constant contact angle θ . Dashed line corresponds to asymmetric shapes relative to the mid-plane between discs.

The procedure is as follows: the radius for the known θ and selected α is computed from

$$r = a(1 \pm \sqrt{1 - \cos \alpha / a^2}) \quad \text{where } a = \frac{\sin \theta (1 + \cos \alpha)}{2} \quad (11)$$

(there are two solutions). After that, the corresponding ϕ that defines the point in the Plateau curve is computed from

$$\phi = \arctg \sqrt{\frac{1 - r^2}{r^2 - \cos^2 \alpha}} \quad (12)$$

(one for each of the two r 's in Eq. 11). Once (α, ϕ) known, the $V/L^3 - S/L^2$ diagram can be computed by means of

$$\begin{aligned} \frac{V}{L^3} &= \frac{v(\alpha, \phi') - v(\alpha, \phi)}{[z(\alpha, \phi') - z(\alpha, \phi)]^3} \\ \frac{S}{L^2} &= \frac{s(\alpha, \phi') - s(\alpha, \phi)}{[z(\alpha, \phi') - z(\alpha, \phi)]^2} \end{aligned} \quad (13)$$

where r, z, v and s are given by Eq. 6 and ϕ' is related to the ϕ given by Eq. 12 in the following way: $\phi' = \phi$ for bulged bridges, $\phi' = -\phi$ for depleted shapes and ϕ' equal to the other value given by Eq. 12 when Eq. 11 is used accordingly (it corresponds to asymmetric bridges).

The limit of stability, i.e. the minimum volume for a stable bridge, is summarized in Figure 9 versus contact angle. The salient features are the minimum volume for $\theta = 0$ ($V/L^3 = 0.98$), that of a catenoidal breakage (that occurs with $\theta = 15^\circ$ and $V/L^3 = 0.77$), that of a cylindrical breakage (that occurs with $\theta = \pi/2$ and $V/L^3 = 1/\pi$, corresponding to $L = \pi R$ as shown in Ref. 5) and the fact that bridge rupture is symmetric for $\theta < 31.1^\circ$ forming two equal drops, and asymmetric for $\theta > 31.1^\circ$, in a similar way as with anchored edges to equal discs.

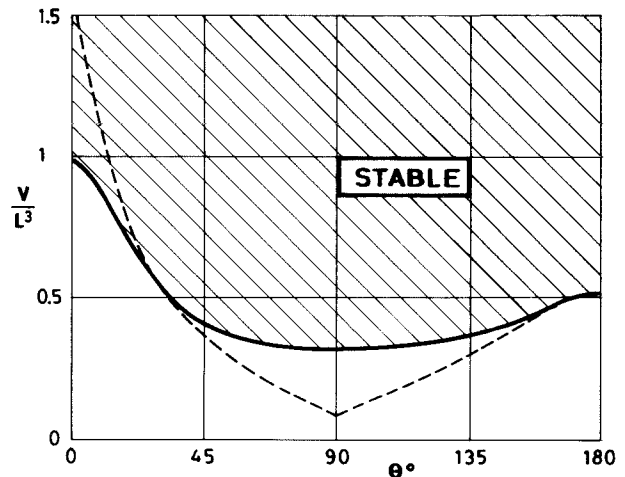


Figure 9. Minimum stable dimensionless volume V/L^3 for a liquid bridge with constant contact angle θ (see Figure 1c).

However, quasi-static evolutions are best followed in Figure 10, where shape variation when liquid is injected or removed is apparent.

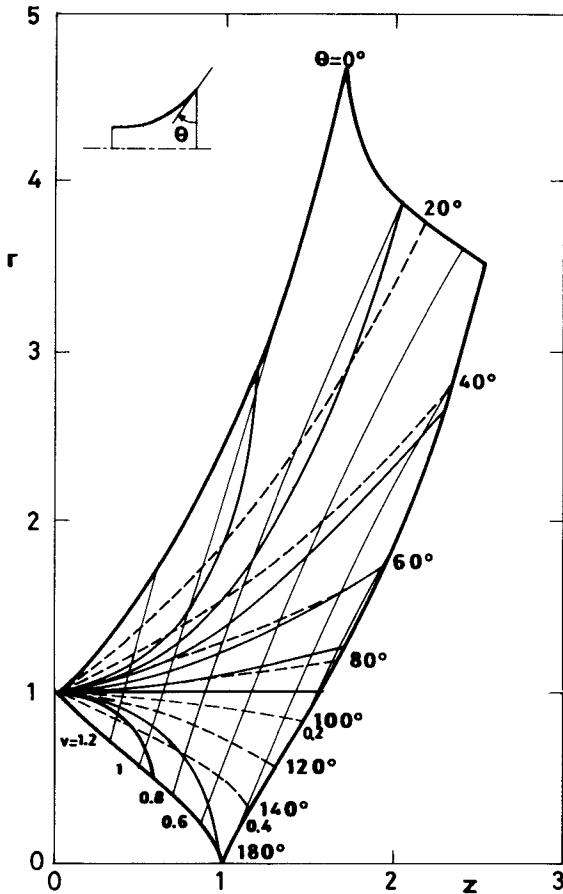


Figure 10. Stability diagram for shapes with constant contact angle θ . For a given θ and a volume $v=V/L^3$, the corresponding thin line gives half of the shape, as shown in the insert. Moving down lines with $\theta=\text{const}$, successive shapes following liquid injection or removal are visualized.

5. PARABOLOIDAL SUPPORTS

An interesting extension of the free-edge problem presented above is to consider curved end-plates as a model for liquid bridges formed in poorly soaked porous media. Convex paraboloidal supports have been included as the easiest approach. In this context, the geometry is specified given the vertex radius R_p of the paraboloids (Figure 1d), the separation L between vertices, the contact angle θ of the interface at the solid boundary and the volume V of liquid. Since θ and R_p are assumed to be fixed, the only two dimensionless parameters to be controlled are L/R_p and V/R_p^3 and, as before, the aim is to work out the stability limit.

As above, the interface shape is best described in terms of the internal variables (α, ϕ) of Plateau's curves (Eq. 6). In that scale the vertex radius r_p of the paraboloid is

$$r_p(\alpha, \phi) = r(\alpha, \phi) \text{tg}[\theta - \gamma(\alpha, \phi)] \quad (14)$$

where r and γ are given by Eq. 6. The expression for L/R_p , V/R_p^3 and S/R_p^2 in this case take the form

$$\left. \begin{aligned} \frac{L}{R_p} &= \frac{z(\alpha, \phi') - z(\alpha, \phi)}{r_p(\alpha, \phi)} - \frac{r^2(\alpha, \phi') + r^2(\alpha, \phi)}{2r_p^2(\alpha, \phi)} \\ \frac{V}{R_p^3} &= \frac{v(\alpha, \phi') - v(\alpha, \phi)}{r_p^3(\alpha, \phi)} - \frac{\pi[r^4(\alpha, \phi') + r^4(\alpha, \phi)]}{4r_p^4(\alpha, \phi)} \\ \frac{S}{R_p^2} &= \frac{s(\alpha, \phi') - s(\alpha, \phi)}{r_p^2(\alpha, \phi)} - \frac{2\pi}{3} \left[\left(1 + \frac{r^2(\alpha, \phi')}{r_p^2(\alpha, \phi)}\right)^{3/2} + \right. \\ &\quad \left. + \left(1 + \frac{r^2(\alpha, \phi)}{r_p^2(\alpha, \phi)}\right)^{3/2} - 2 \right] \end{aligned} \right\} (15)$$

where last terms account for the effect of the immersed tip of paraboloids.

Following the same procedure detailed above for unequal discs, the following results have been obtained. Long bridges break in an asymmetric way when the shape approaches a complete period of Plateau's curves, being it applicable to liquids with large (say $\theta > 45^\circ$) contact angles to the solid supports. In particular, cylindrical zones, formed when the liquid volume is the appropriate for the interface to reach the point where the paraboloidal shape matches the contact angle, break at $L=2\pi R$, though the volume is less than $\pi R^2 L$ due to the protruding paraboloidal tips (line a in Figure 11). Short zones, normally found with small contact angles, break in a symmetric way. The stability limits for configurations with contact angle 30° , 60° or 90° are drawn in Figure 11, where point A, separating symmetric breakage (for $L < L_A$) from asymmetric one ($L > L_A$) is seen in the case of 60° ; for 30° it is beyond the limits shown, and for 90° it shifts to the origin.

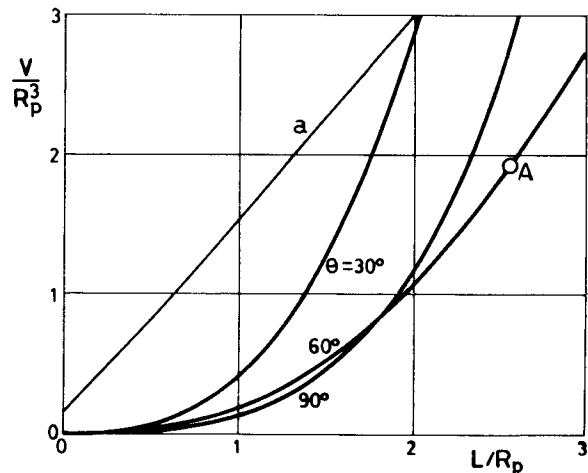


Figure 11. Stability limits for liquid bridges with constant contact-angle θ between paraboloidal supports. For $\theta=60^\circ$ line a corresponds to cylindrical shapes, separating the upper region of bulged shapes from the lower one of spindled shapes. Point A separates symmetric (below) and asymmetric (above) modes of breaking.

6. CONCLUSIONS

The first step in the understanding of fluid-interface behaviour is to locate the interface shape, performing equilibrium and stability analysis, what has been done here for some interesting bridge configurations. As a general conclusion, long zones loose their stability through an asymmetric mode and yield two distinct drops, whereas short zones tend to neck in a symmetric way and yield similar drops. As expected, imperfections imposed to equal-disc bridges introduce deviations in the behaviour of such bridges that have very similar consequences: reduction of the stability limits, bias in the otherwise symmetric structure, etc.

When the bridge has not its borders anchored to sharp solid edges, the stability limits reduce nearly to a half (in achievable slenderness, for instance). Practical problems associated with the advancing and receding contact lines, however, seem to put in question the validity of results for free-contact-line bridges.

This work has been sponsored by the Spanish Commission for Space Research (CONIE).

1. Martínez I 1978, Floating zone: equilibrium shapes and stability criteria, *COSPAR Space Research XVIII*, 519-522.
2. Martínez I 1978, Hidrostática de la zona flotante, *Tesis Doctoral*, Universidad Politécnica de Madrid.
3. Vega J M & Perales J M 1983, Almost-cylindrical isorotating liquid bridges for small Bond numbers, in *ESA SP-191*.
4. Da Riva I & Martínez I 1979, Floating zone stability (Exp. 1-ES-331), *ESA SP-142*, 67-74.
5. Boucher E A & Evans M J B 1980, Properties of fluid bridges between solids in a gravitational field, *J. Colloid Interf. Sci.*, 75, 409-418.
6. Martínez I 1976, Floating zone under reduced gravity: axisymmetric equilibrium shapes, *ESA SP-114*, 277-282.